Soft Matter

PAPER

Cite this: *Soft Matter*, 2020, **16**, 2301

PEGylated gene carriers in serum under shear flow†

Dongxiao Yin,[a] Hao Wen,[a] Guangqi Wu,[a] Shaolu Li,[a] Chenyang Liu,[b] Hua Lu *[a] and Dehai Liang *[a]

Received 5th December 2019,
Accepted 19th January 2020

DOI: 10.1039/c9sm02397f

rsc.li/soft-matter-journal

The behaviour of drug/gene carriers in the blood stream under shear is still a puzzle. In this work, using the complexes formed by 21 bp DNA and poly(ethylene glycol)-*b*-poly(L-lysine) (PEG–PLL) of varying PEG lengths, we studied the dynamic behaviour of the complexes in the presence of fetal bovine serum (FBS) and under flow at different shear rates, a condition mimicking the internal physical environment of blood vessels. The PEG_{5k}-PLL/DNA complex possesses a dense DNA/PLL core and a loose PEG_{5k} protecting layer. The PEGylated DNA complexes exhibit multiple responses to external shear in the presence of FBS. The loose PEG_{5k} layer is firstly disturbed at a shear rate below 30 s^{-1}. The exposure of the charged core to the environment results in a secondary aggregation of the complex with FBS. The size of the aggregate is limited to a certain range as the shear rate increases to 50 s^{-1}. The dense DNA/PLL core starts to withstand the shear force as the shear rate reaches 500 s^{-1}. The reorganization of the core to accommodate more serum molecules leads to tertiary aggregation of the complexes. If PEG cannot form a valid layer around the complex, as in PEG_{2k}-PLL/DNA, the complex forms an aggregate even without shear, and the first shear dependent region is missing. If the PEG layer is too stable around the complex, as in PEG_{10k}-PLL/DNA, no tertiary aggregation occurs. The mechanism of shear on the behaviour of delivery particles in serum helps to design gene carriers with high efficacy.

Introduction

Gene carriers, including viral and non-viral vectors, have been developed to treat incurable diseases, such as cancer and hereditary diseases.[1–8] A polycation, as a classic non-viral vector, can condense nucleic acids *via* electrostatic interaction and protect them from degradation under physiological conditions.[9–17] In consideration of many unfavourable physiological obstacles, the properties of the complexes formed by polycations and nucleic acids need to be designed carefully. For example, the carriers are generally coated with a layer of polyethylene glycol (PEG) to increase the circulation time in the blood stream and to lower the toxicity[13,18,19] A ligand is introduced on the surface of the carrier to achieve targeting to specific cells.[20,21] The +/− charge ratio of the complex is larger than unity to facilitate the interaction with the negatively charged cell membrane.[22–25] Moreover, the size and shape of the particles,[26–28] the structure of the polycations,[4,29,30] and other parameters are able to enhance the performance of the carriers. However, it is still hard to establish a definite relationship between the physicochemical properties of the carrier and the transfection efficacy *in vivo*. One reason for this is that the behaviour of the carrier is hard to monitor and predict in a biological system, which is complicated and always far from thermodynamic equilibrium.

After being administrated intravenously, the gene carriers firstly encounter the blood stream. It is reported that the positively charged carriers form large aggregates with the components in the serum, deteriorating the therapeutic performance.[31,32] Moreover, the shear force caused by blood flow also exhibits a strong effect on the shape and structure of the administrated particles. In a healthy body, the shear rate of blood flow ranges from 20 s^{-1} to 2000 s^{-1}, and it can reach up to 10^5 s^{-1} in some extreme conditions, like in patients with carotid stenosis.[33,34] It has been reported that some serum components are sensitive to blood flow. For example, the unfolding of von Willebrand factor, which is related to platelet aggregation and thrombus formation, is induced by shear.[35,36] Both experiments and theoretical studies have been applied to understand the micro-mechanics and to predict the behaviour of particles under shear stress.[37–41] Zanina *et al.* reported that a swollen hydrogel was deformed and it released water in silicon oil under shear.[37] The breakage of large vesicles in shear flow was observed by

[a] *Beijing National Laboratory for Molecular Sciences and the Key Laboratory of Polymer Chemistry and Physics of Ministry of Education, College of Chemistry and Molecular Engineering, Peking University, Beijing 100871, China. E-mail: chemhualu@pku.edu.cn, dliang@pku.edu.cn*

[b] *Beijing National Laboratory for Molecular Sciences, Institute of Chemistry, Chinese Academy of Sciences, Beijing 100190, China*

† Electronic supplementary information (ESI) available. See DOI: 10.1039/c9sm02397f

Pal *et al.*[38] Theoretical studies showed that soft, elastic particles in an unbounded simple shear flow exhibited steady-state, trembling, or tumbling depending on the shear rate, elastic shear modulus, and initial particle shape.[39,40] Takeda *et al.* reported that the structure of the polyplex micelles formed by nucleic acids and polycations was deteriorated when exposed to shear stress, which lowered the delivery efficiency.[15] The micelles formed by the block copolymer of PEG with either poly(ε-caprolactone) or poly(D,L-lactide) quickly dissociated in the presence of serum under blood shear flow.[42] In previous work, we investigated the effect of shear force on the complex formed by DNA with K20 (K: Lysine), protamine, and poly(L-lysine) (PLL), separately, in the presence of serums.[43] A critical shear rate exists for each system. Below the critical value, the shear mainly shows stirring effects, leading to the secondary aggregation of complexes; while it serves as a mechanical force to break down the complex into smaller size particles above the critical value. A model study indicates that the critical shear rate is related to the surface tension, the chain density, and the elasticity of the complexes.[43]

As mentioned above, the gene carriers are generally coated with a protecting layer, such as PEG,[18,31,44] sugar molecules,[14,45] or zwitterions,[46–48] to prevent the aggregation in the blood stream. Compared with the dense core of the carrier, the protecting layer generally possesses a lower chain density and surface tension. Therefore, the dynamics of the protecting layer in the shear flow should be different from the core of the carrier. Knowing the behaviour of such carriers in the blood stream is crucial to reveal at least partially the parameters affecting the transfection efficiencies *in vivo*. It is also helpful to design the gene carriers capable of overcoming the barriers in the blood stream. In this work, using the complexes formed by PEG–PLL and DNA as an example, we systematically study the effect of shear on the structure of the complexes with a protecting layer. A rheometer with a double-gap Couette is used to mimic the physiological conditions in the blood stream and apply shear stress on a DNA complex in the presence of serum. Laser light scattering (LLS) is employed to study the size and dynamics of the DNA complex after shear treatment. Compared to that of the complexes without a PEG layer, the behaviour of PEG–PLL/DNA is more complicated when exposed to flow at different shear rates. The loose PEG layer is disturbed at a lower shear rate, while the critical shear rate for the dense core of the complex is much higher. Therefore, the complex undergoes a sequence of secondary aggregation, breaking into small size pieces, reorganization, and tertiary aggregation with increasing shear rate from 30 s^{-1} to 3000 s^{-1}. These behaviours also depend on the length of PEG. Besides, the shear time exhibits a similar effect to the shear rate.

Materials and methods

Materials and sample preparation

mPEG-NH_2 samples with different molecular weights (2k Da, 5k Da and 10k Da) were purchased from Shenzhen Meiluo Technology Co., Ltd (China). PEG–PLL was synthesized by following a known procedure.[49] PEG–PLL(Z) was obtained from the ring-opening polymerization of Lys(Z)-NCA using PEG-NH_2 as an initiator, and then PEG–PLL was obtained by the deprotection of PEG–PLL(Z) using HBr/HAc. The successful synthesis of PEG–PLL(Z) and PEG–PLL was validated by proton NMR spectroscopy. The average number of lysine was determined to be 22 ± 1. The resulting copolymers are thus named as PEG_{2k}-PLL, PEG_{5k}-PLL, and PEG_{10k}-PLL. Fetal Bovine Serum (FBS) was purchased from M&C Gene Technology Ltd. (Beijing, China). Dulbecco's phosphate-buffered saline (DPBS) and complementary 21 nt oligonucleotide strands with random sequence were purchased from Invitrogen Inc (Shanghai, China). Stock solution of 21 bp oligonucleotide at 1.0×10^{-3} g mL^{-1} was obtained by mixing the complementary strands with a stoichiometric ratio in DPBS buffer, heating to 95 °C for 5 min, and then annealing to room temperature. All PEG–PLL samples (0.1 g L^{-1}), DNA (0.5 g L^{-1}), and 10% FBS were prepared in DPBS buffer and stored at 4 °C prior to use. Known amounts of DNA solution were added to the PLL-PEG solution (1.0 mL) to obtain the complex at different +/− ratios (+/− ratio, the molar charge ratio, stands for the number of positively charged amino groups from all the polycations to the number of negatively charged phosphate groups from all the dsDNA). The moment of mixing is set as the starting point. To prepare the complex/FBS aggregates, the complex was gently shaken for 30 seconds and equilibrated for 30 minutes before mixing with the same volume of 10% FBS. All the reagents including FBS were filtered to remove dust before mixing.

Polyelectrolyte complexes/FBS aggregates under shear

Shear stress was generated by an MCR301 rheometer (Anton Paar, Graz, Austria) equipped with double-gap Couette geometry. The mixture of DNA complex and FBS solution was loaded into the Couette and treated under steady shear at a chosen shear rate for a known time period. Dust was removed from all the reagents and Couette beforehand. The sample was taken out using a pipette for AFM and LLS experiments at specifically chosen time points.

Laser light scattering (LLS)

A commercialized spectrometer from Brookhaven Instrument Corporation (BI-200SM Goniometer, Holtsville, NY) was used to perform both static light scattering (SLS) and dynamic light scattering (DLS) over a scattering angular range of 20–150°. A vertically polarized, 17 mW He–Ne laser (Research Electro Optics, Inc. Colorado, USA) operating at 633 nm was used as the light source.

In static light scattering (SLS), the angular dependence of the excess absolute time-averaged scattered intensity, known as the Rayleigh ratio $R_{vv}(\theta)$ (θ is the angular degree), was measured. For a very dilute solution, the weight-averaged molar mass (M_w) and the root mean-square radius of gyration (R_g) can be obtained on the basis of the equation:

$$\frac{HC}{R_{vv}(\theta)} = \frac{1}{M_w}\left(1 + \frac{1}{3}R_g^2 q^2\right) + 2A_2C \quad (1)$$

where $H = 4\pi^2 n^2 (dn/dc)^2/(N_A/\lambda^4)$ and $q = 4\pi n/\lambda \sin(\theta/2)$ with N_A, n, dn/dc, and λ being Avogadro's number, the solvent refractive index, the specific refractive index increment, and the wavelength of light in a vacuum, respectively. If the system contains more than one component, eqn (1) is not applicable to determine the molecular weight. The excess scattered intensity I_{ex} is used instead to show the formation of larger size aggregates. The I_{ex} at angle θ is calculated by

$$I_{ex}(\theta) = \frac{I_s(\theta) - I_0(\theta)}{I_t(\theta)} \quad (2)$$

with $I_s(\theta)$, $I_0(\theta)$, and $I_t(\theta)$ being the scattered intensity from the solution, the solvent, and toluene, respectively. I_{ex} at 30° is used for comparison if the sample changes with time.

In dynamic light scattering (DLS), the intensity–intensity time correlation function $G^{(2)}(\tau)$ in the self-beating mode was measured. A correlation curve is obtained in 1 minute. A Laplace inversion program, CONTIN, was used to process the data to obtain the line width distribution and the diffusion coefficient D. The diffusion coefficient can be further converted into the hydrodynamic radius R_h by using the Stokes–Einstein equation:

$$D = \frac{k_B T}{6\pi\eta R_h} \quad (3)$$

where k_B, T, and η are the Boltzmann constant, the absolute temperature, and the viscosity of the solvent, respectively.

Atomic force microscopy (AFM)

AFM measurements were conducted in the ScanAnalyst-Air mode on a Dimension Icon Atomic Force Microscope (Bruker, USA). The data were collected in air by a commercial silicon tip (SI-DF3, Seiko instruments Inc.). 20–30 μL of the sample solution was deposited and kept standing for 40 seconds on a fresh mica surface. The excess solution was then blotted away with a strip of filter paper, and the mica surface was washed with 30–40 μL of deionized water to remove the salt. The sample was air-dried for one day before AFM experiments.

Results and discussion

PEG–PLL/DNA complexes and their behaviour in FBS

The polycation-based gene carrier generally exhibits prominent transfection efficiency when the +/− ratio of the complex is above 5 or higher, under which condition the electrostatic interaction between the complex and the membrane facilitates the cellular uptake.[22] We firstly chose PEG_{5k}-PLL and studied the stability of DNA complexes at +/− ratios of 5, 10, and 20, separately. At all the studied charge ratios, the complexes undergo a slow aggregation process with time, as demonstrated by the excess scattered intensity I_{ex} (Fig. 1A). The appearance of a bi-modal distribution (Fig. 1B–D), with a larger peak (+/− = 10, 20) or both peaks (+/− = 5.0) representing the aggregates, also confirms this conclusion. The aggregation process is also dependent on the charge ratio. The complex at +/− = 20 is relatively more stable than that at +/− ratio of 5 or 10, as indicated by the weaker growth of the size and the excess scattered intensity under the same conditions. These results suggest that the protection of the complex from further aggregation by hydrophilic PEG corona is highly dynamic. The protection is more effective if the amount of PEG is large enough, *e.g.* at +/− = 20. This conclusion is further supported by the stability of the complexes formed by DNA and PEG–PLL of varying PEG lengths. At fixed +/− = 20, PEG_{10K}-PLL offers the best protection on the DNA complex, as demonstrated by the smallest and yet stable size (Fig. 2c), as well as the excess scattered intensity (Fig. 2d). In contrast, the PEG_{2k}-PLL/DNA complex, which is insufficiently protected by short PEG chains, exhibits a fast increase in size (Fig. 2a) and in excess scattered intensity (Fig. 2d) due to the formation of aggregates.

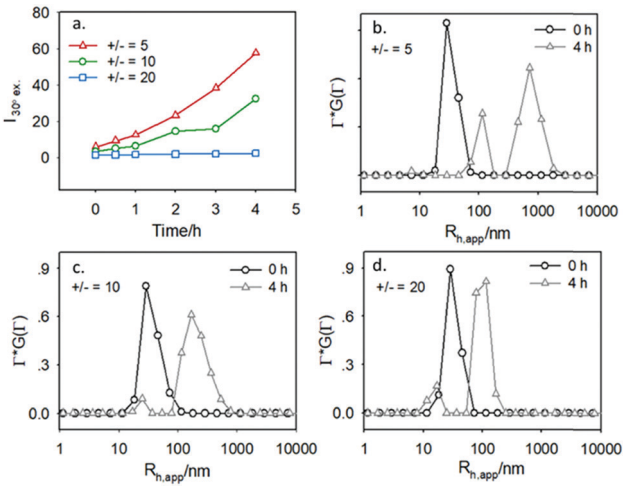

Fig. 1 PEG_{5k}-PLL/DNA complex at different +/− ratios. Time dependence of I_{ex} (A), size distributions of the complex at +/− ratios of 5 (B), 10 (C), and 20 (D). Scattered angle: 30°.

The complex at +/− = 20 is chosen for the following studies. We firstly investigate their behaviour in the presence of serum. 5% serum itself exhibits multi-modal distribution with the size

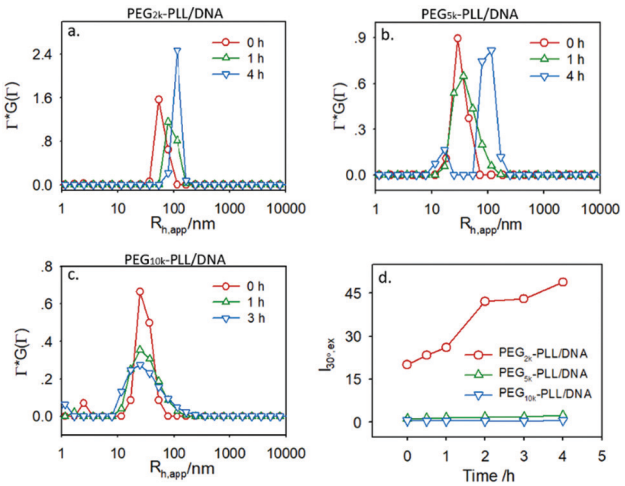

Fig. 2 Time dependence of size distribution of the complexes formed by DNA with (a) PEG_{2k}-PLL, (b) PEG_{5k}-PLL, and (c) PEG_{10K}-PLL, as well as the changes in I_{ex} (d). Charge ratio +/− = 20, scattered angle: 30°.

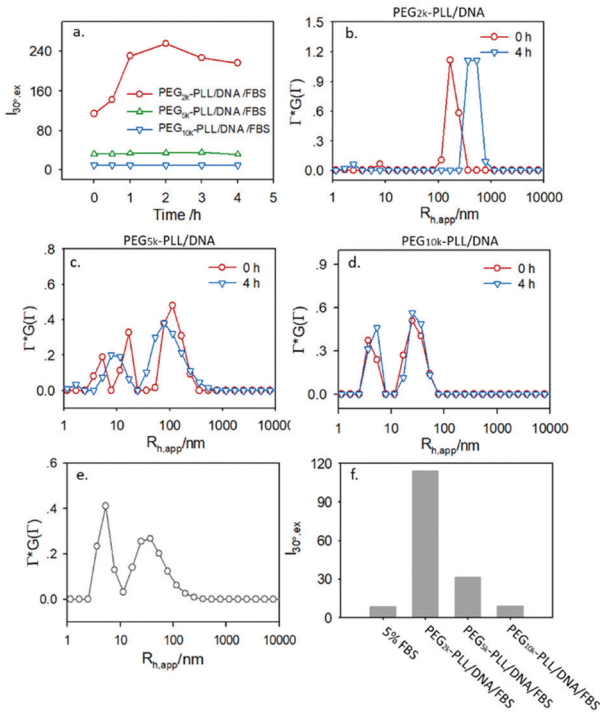

Fig. 3 LLS results on the PEG–PLL/DNA complexes in the presence of 5% FBS. Time dependence of the excess scattered intensity (a) and size distribution of complex formed by DNA with PEG_{2k}-PLL (b), PEG_{5k}-PLL (c), and PEG_{10k}-PLL (d), separately. (e) The size distribution of 5% FBS, and (f) the comparison of the excess scattered intensity of 5% FBS, and the complexes formed by different PEG–PLL. The +/− ratio of the PEG–PLL/DNA complex is 20. Scattered angle: 30°.

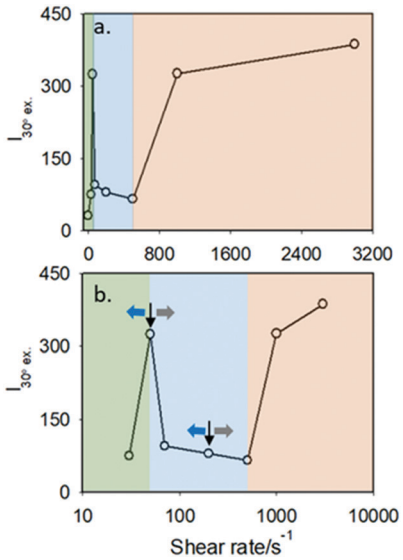

Fig. 4 Shear rate dependence of I_{ex} of PEG_{5k}-PLL/DNA/FBS after being sheared for 2 h (a). The plot with x-axis in the logarithmic scale is shown in (b). The black arrows indicate the data points at shear rates of 50 and 200 s^{-1}. The +/− ratio of the PEG–PLL/DNA complex is 20. Scattering angle: 30°.

below 20 nm (Fig. 3e). It is reasonable because the serum contains a variety of components other than albumin. The association or aggregation of the components, which is more severe at high concentrations, leads to a multimodal size distribution.[50] When FBS is mixed with the complexes, the negatively charged components in serum, such as albumin, can further interact with the complex if it is not well protected. Since the corona formed by PEG_{2K} is not sufficient to ensure even the stability of PEG_{2k}-PLL/DNA complex itself (Fig. 2), larger size aggregates are formed instantly in the presence of FBS. The peaks corresponding to free serum components disappear and the $R_{h,app}$ of the aggregates reaches about ~470 nm in 4 h (Fig. 3b). The I_{ex} increases in the first two hours and then starts to decline due to the formation of precipitates (Fig. 3a), a typical behaviour of the PLL/DNA complex interacting with serum components.[51] The PEG_{10k}-PLL/DNA complex is well-protected by the long chain PEG_{10k} and no prominent aggregation is formed in serum (Fig. 3d), which is further demonstrated by the weak yet stable I_{ex} (Fig. 3a and f). The PEG_{5k}-PLL/DNA complex is also stable in the presence of 5% FBS. The I_{ex} exhibits a limited increase (Fig. 3f) and the size distribution is relatively stable in the studied time period (Fig. 3c).

PEG_{5k}-PLL/DNA complex at different shear rates

The behaviour of the complexes in the presence of FBS is quite sensitive to shear rate. Using the PEG_{5k}-PLL/DNA/FBS complex as the sample, we treated it for 2 h at different shear rates ranging from 30 s^{-1} to 3000 s^{-1}, and then studied the changes by LLS. The shear rate dependence of the excess scattered intensity is shown in Fig. 4. The curve can be divided into three regions: (i) the increase of intensity at $\dot{\gamma} \leq 50\ s^{-1}$; (ii) the relatively stable region with low intensity at $70\ s^{-1} \leq \dot{\gamma} \leq 500\ s^{-1}$; and (iii) the secondary increase of intensity at $\dot{\gamma} > 500\ s^{-1}$.

The size distributions at different shear rates are compared in Fig. 5. The PEG_{5k}-PLL/DNA complex in the presence of the serum exhibits a multimodal distribution when sheared at 30 s^{-1} for 2 h. Besides the serum (two small peaks with size below 20 nm) and the aggregates of PEG_{5k}-PLL/DNA with serum (around 100 nm), an extra mode with a size of around 500 nm is observed in the system (Fig. 5a), which indicates the formation of another kind of aggregate. The size of this giant aggregate is almost doubled when the sample is treated at 50 s^{-1} for 2 h (Fig. 5b). Meanwhile, the peaks around 10 nm and 100 nm are largely reduced, suggesting that the giant aggregates result from further interaction between the complex and serum. Since the excess scattered intensity is proportional to the sixth power of the particle size, the change in the size and the ratio of the giant aggregate accounts for the sharp increase in the excess scattered intensity (Fig. 4). At 70 s^{-1}, however, the size of the giant aggregate reduces to 360 nm, while the other one is only 30 nm (Fig. 5c). The ratio of the giant aggregate also decreases. Both results explain the declination of the excess scattered intensity. The size distributions are similar at a shear rate ranging from 70 s^{-1} to 500 s^{-1} (Fig. 5c–e). By further increasing the shear rate to 1000 s^{-1} or 3000 s^{-1}, the giant aggregate increases again at the cost of the smaller size components (Fig. 5f and g). The shear rate dependence of the size distribution is in agreement with that of the excess scattered intensity in this stage (Fig. 4).

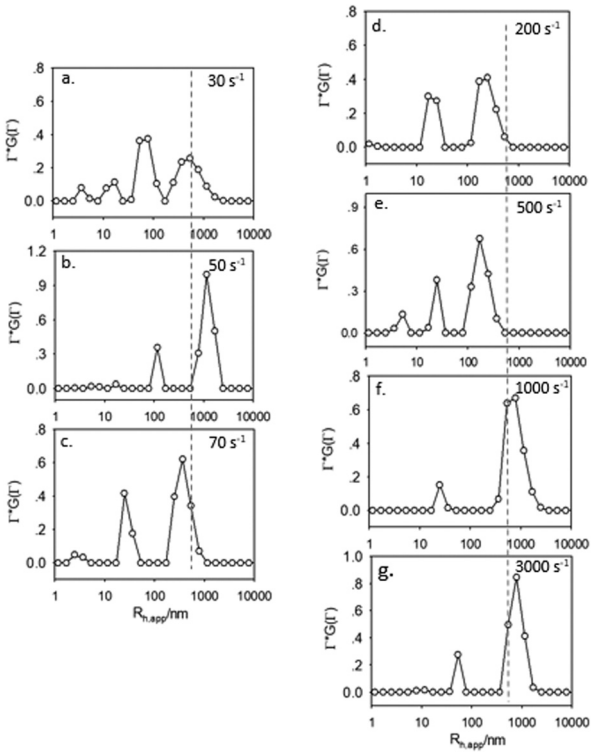

Fig. 5 Size distribution of PEG_{5k}-PLL/DNA/FBS after being sheared for 2 h at shear rates of (a) 30 s^{-1}, (b) 50 s^{-1}, (c) 70 s^{-1}, (d) 200 s^{-1}, (e) 500 s^{-1}, (f) 1000 s^{-1}, and (g) 3000 s^{-1}. The dotted vertical line shows the size of 533 nm. Scattered angle: 30°.

AFM experiments were conducted to determine the morphologies of the PEG_{5k}-PLL/DNA/FBS complexes after being sheared for two hours. The complexes and their aggregates exhibit mainly an aspheric shape after being dried on the mica surface. The spheres could further aggregate into clusters, *e.g.* at 30 s^{-1} or 200 s^{-1}. With increasing $\dot{\gamma}$ from 30 s^{-1} to 50 s^{-1}, the size or height of the complexes sharply increases (Fig. 6a and b). As the shear rate increases for the second region, *e.g.*, 200 s^{-1}, the average size of the aggregates decreases (Fig. 6c). When $\dot{\gamma}$ reaches 1000 s^{-1}, the average size of the particles increases again in the system (Fig. 6d). The particle size as determined by AFM in each region is in accordance with the LLS result (Fig. 4).

Effect of shear time

The effect of shear could be controlled not only by shear rate, but also by shear time. Both DLS and AFM images show that the treatment of the PEG_{5k}-PLL/DNA/FBS complex at 50 s^{-1} for 2 h yields a peak excess scattered intensity and a maximum size (Fig. 4 and 6). Fixing the shear rate at 50 s^{-1}, we treated the PEG_{5k}-PLL/DNA/FBS for 1 h and 4 h, separately. Interestingly, the size of the giant aggregate shrinks after both the 1 h treatment (Fig. 7a) and 4 h treatment (Fig. 7c). The decrease in the excess scattered intensity also confirms this conclusion (Fig. 8a). These results suggest that at least two parameters with the opposite effect on the aggregation of the complexes exist under shear.

The size and the excess scattered intensity of the PEG_{5k}-PLL/DNA/FBS complex after being sheared for 2 h is low in the 70 $s^{-1} \leq \dot{\gamma} \leq$ 500 s^{-1} region (Fig. 4). The complex treated at 200 s^{-1} is also chosen to study the effect of the shear time. Results show that the complex exhibits a larger size (Fig. 7d and f) and higher excess scattered intensity (Fig. 8b) as the shear time is shortened to 1 h or increases to 4 h, in contrast to the behaviour at 50 s^{-1}.

AFM images show similar results as LLS. Compared with the particle treated for 2 h, the size or height of the particles are larger or in a fused state after being treated for 1 h or 4 h at 200 s^{-1} (Fig. 9d–f), while the opposite trend is observed at 50 s^{-1} (Fig. 9a–c). The plot of the excess scattered intensity *versus* shear rate (Fig. 4) clearly indicates that longer shear time generates similar effects to higher shear rate, as indicated by the grey arrows, while a shorter shear time generates a similar effect to the lower shear rate, as indicated by the blue arrows.

Effect of PEG chain length

Since the length of PEG is closely related to the stability of the PEG–PLL/DNA complex in serum (Fig. 3), it is a key parameter determining the behavior of the complex under shear. The PEG_{2k}-PLL/DNA complex itself is not stable in the presence of serum because of the insufficient protection by the short length PEG (Fig. 3a and b). When shear is applied, the large aggregate

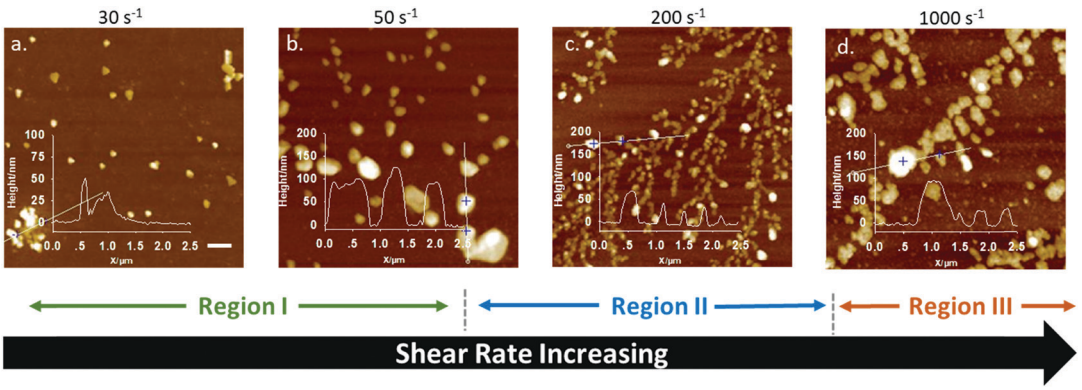

Fig. 6 AFM images and the corresponding height profile (inset) of PEG_{5k}-PLL/DNA/FBS after shearing for 2 h at (a) 30 s^{-1}, (b) 50 s^{-1}, (c) 200 s^{-1}, (d) 1000 s^{-1}. Scale bar: 500 nm.

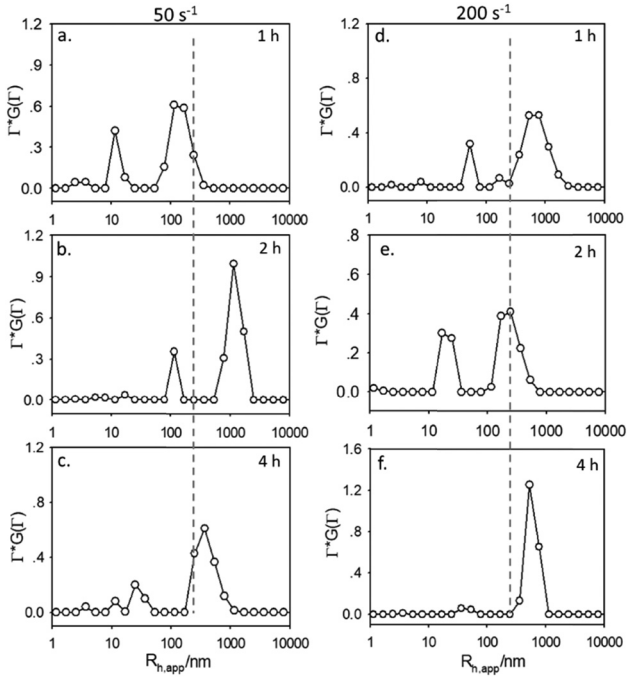

Fig. 7 Size distribution of PEG_{5k}-PLL/DNA/FBS after being sheared at 50 s^{-1} (a–c) and 200 s^{-1} (d–f), separately, for 1 h, 2 h, and 4 h. The dot vertical line shows the size of 250 nm. Scattered angle: 30°.

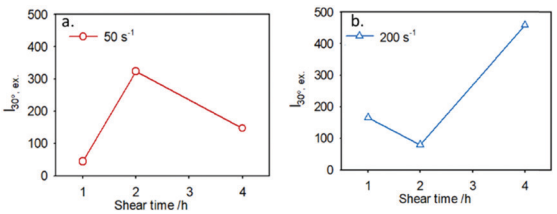

Fig. 8 (a) and (b) show the shear time dependence of I_{ex} at 50 s^{-1} and 200 s^{-1}, respectively. Scattered angle: 30°.

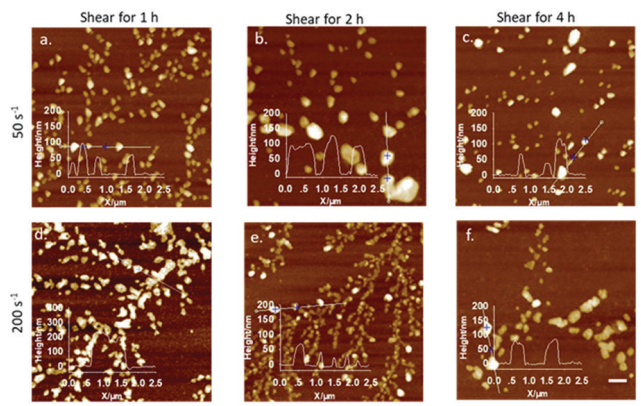

Fig. 9 AFM images and the corresponding height profile (inset) of PEG_{5k}-PLL/DNA/FBS after being sheared at (A) 50 s^{-1} and (B) 200 s^{-1}, separately, for 1 h, 2 h, and 4 h. Scale bar: 500 nm.

breaks down (Fig. 11a) even at very low shear rate ($\dot{\gamma}$ = 30 s^{-1}). The size of the aggregate remains constant and then starts to

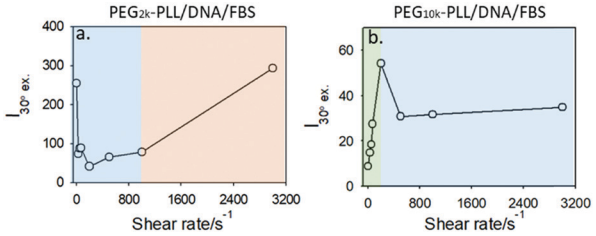

Fig. 10 Shear rate dependence of I_{ex} of PEG_{2k}-PLL/DNA/FBS (a) and PEG_{10k}-PLL/DNA/FBS (b) after being sheared for 2 h. The +/− ratio of the PEG–PLL/DNA complex is 20. Scattering angle: 30°.

decrease at 200 s^{-1}. It reaches the minimum at 1000 s^{-1} and begins to increase (Fig. 11b–f). The plot of I_{ex}, which sharply drops at the beginning, becomes relatively stable at the intermediate region, and increases after 1000 s^{-1} (Fig. 10), which agrees with the changes in size. Compared with the three regions of the PEG_{5k}-PLL/DNA complex at different shear rates (Fig. 4), only the last two regions are observed in the PEG_{2k}-PLL/DNA complex since it already forms large aggregates at the initial conditions.

In the case of the PEG_{10k}-PLL/DNA complex, which is well protected by the long chain PEG_{10k}, only the first two regions are observed in the studied shear rate range. Similar to the behaviour of the PEG_{5k}-PLL/DNA complex, the PEG_{10k}-PLL/DNA complex forms aggregation as the shear at 30 s^{-1} is applied (Fig. 11h). As the shear rate increases, the ratio of FBS continually decreases accompanied with an increase of the aggregate (Fig. 11h–k), suggesting that more serum components form aggregates with the PEG_{10k}-PLL/DNA complex. The change in I_{ex} (Fig. 10b) also confirms this trend. The first shear rate region of PEG_{10k}-PLL/DNA/FBS prolongs to $\dot{\gamma}$ = 200 s^{-1}, much broader than that of PEG_{5k}-PLL/DNA/FBS. At shear rates above 200 s^{-1}, the PEG_{10k}-PLL/DNA/FBS system enters the second region, in which both I_{ex} and the size of the aggregates exhibit a sharp decrease and then become relatively stable. No onset is observed even at 3000 s^{-1}.

The morphologies of the PEG_{2k}-PLL/DNA complex and PEG_{10k}-PLL/DNA complex in the presence of FBS after being sheared in different regions are also determined by AFM. Most of them are in spherical shapes, while the ellipsoidal aggregates are also observed (Fig. 12). For PEG_{2k}-PLL/DNA/FBS, the particle size decreases with increasing shear rate at a lower shear rate region, and a slight recovery of the particle size occurs at an extremely high shear rate (Fig. 12a–c). In the case of PEG_{10k}-PLL/DNA/FBS, the size of the aggregates increases with the shear rate in the first region (Fig. 12d and e), and an opposite trend is observed with further increasing shear rate even to 3000 s^{-1} in the second region (Fig. 12f).

Mechanism of shear effect on DNA complex

Our previous study on the PLL/DNA complex demonstrated that the shear generates two effects: a mechanical force to break down the complex into smaller size particles above a critical shear rate and a stirring effect leading to secondary aggregation of complexes below the critical shear rate.[43] The critical shear

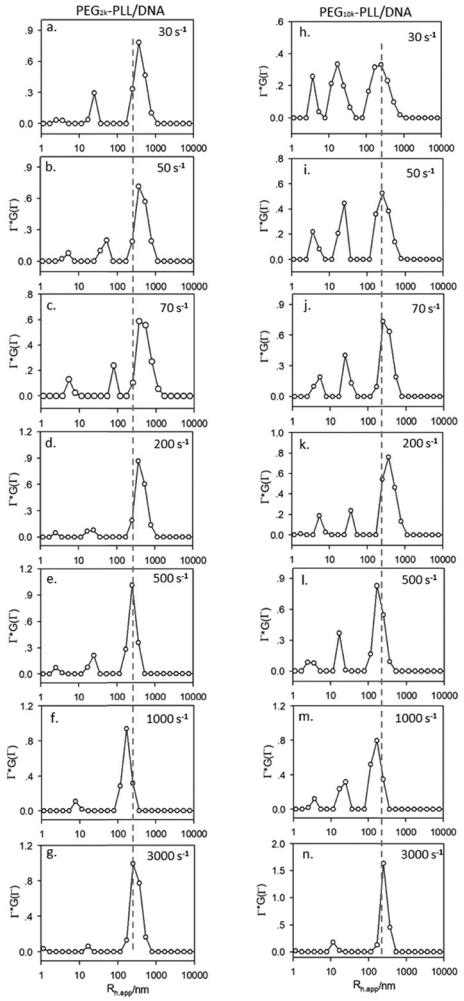

Fig. 11 Size distribution of PEG_{2k}-PLL/DNA/FBS (a–g) and PEG_{10k}-PLL/DNA/FBS (h–n) after being sheared for 2 h at a shear rate of 30 s^{-1}, 50 s^{-1}, 70 s^{-1}, 200 s^{-1}, 500 s^{-1},1000 s^{-1}, and 3000 s^{-1} respectively. The dot vertical line shows the size of 250 nm. Scattered angle: 30°.

rate is determined by the intrinsic property of the particle, especially the density, surface tension, and viscoelasticity. The PEG–PLL/DNA complex is different from the PLL/DNA complex in that the former contains a dense PLL/DNA core and a loose PEG protecting layer. The core and the layer respond differently to the shear rate/shear time. The PEG–PLL/DNA complex can further form aggregates in serum if the PEG corona or the dense PLL/DNA core is disturbed or deformed. Moreover, the size of aggregates is also sensitive to the shear rate. Therefore, for either the corona or the core, there exist two critical shear rates: one starts to disturb the corona/core and the other limits the formed aggregate to an optimal size. The dependence of shear time is due to the viscoelasticity of complexes or aggregates.

The PEG_{5k}-PLL/DNA complex exhibits three regions in the presence of serum with increasing shear rates. As schematically shown in Fig. 13, the outer PEG layer firstly experiences from a mechanical force along the streamline as the shear is applied. The critical shear rate to disturb the loose PEG_{5k} layer could be very low, below 30 s^{-1}, which is not determined in this study. The disturbance of the PEG protecting layer partially exposes the DNA/PLL core to the environment full of serum (Fig. 13a). A secondary aggregation (Fig. 13b) occurs. The serum mainly interacts with the complex at the interface between the core and the corona at this stage. The increase in the size continues until the shear rate reaches another critical value to prevent the aggregate from growing. The critical shear rate for the PEG_{5k}-PLL/DNA complex is 50 s^{-1}, after which the size of the aggregates is limited to a smaller value in this region. Shear force could change the shape of the particles. The degree of deformation is proportional to the capillary number $C_a = \eta\dot{\gamma}/G$, where η is the shear viscosity of fluid and G is the shear elastic modulus of particles. Thus, further increasing the shear rate or shear time results in heavy deformation of the complex particles.[39] The dense DNA/PLL core starts to withstand the shear force as the shear rate reaches a critical value, which is about 500 s^{-1} for the PEG_{5k}-PLL/DNA complex. The relaxation of the DNA or PLL inside the complex releases the unneutralized segments or loops induced by shear, which results in further aggregation not only between the serum and the complex, but also between different complexes. Together with a full exposure of the entire core to the environment, heavy aggregation occurs again (Fig. 13d). By further increasing the shear rate to a certain value, the size of the aggregates should decrease due to its limitation effect. This shear rate value is more than 3000 s^{-1}, beyond the range of the rheometer.

The PEG_{2k}-PLL/DNA complex forms large aggregates with the serum due to the insufficient protection of PEG_{2k}. Therefore, the initial stage of the PEG_{2k}-PLL/DNA complex starts from the beginning of the second stage (Fig. 13b) as the shear is applied. In contrast, the PEG_{10k}-PLL/DNA complex is well-protected by PEG_{10k} in serum. The disturbance of PEG_{10k} corona which results in the formation shown in Fig. 13b occurs at a higher shear rate. Therefore, the first shear rate dependent region is prolonged in the PEG_{10k}-PLL/DNA/FBS system. Since PEG_{10k} is much longer than the length of DNA, which is only 21 bp, the DNA/PLL core in the PEG_{10k}-PLL/DNA complex is close to equilibrium due to the interference of PEG_{10k}. No prominent aggregation (Fig. 13d) occurs as the core is disturbed. Therefore, the third region goes missing. As 21 bp DNA is replaced by the long chain salmon DNA (~2000 bp) to enhance the DNA/PLL core, three regions are clearly observed in the studied shear rate range (Fig. S1 and S2, ESI†).

The shear treatment disturbs the PEG corona at a lower shear rate and the cores of the complex at a higher shear rate, both of which deteriorate the stability of the PEG–PLL/DNA complex in FBS. Precipitates are generally observable within 24 h after shear treatment, especially for the complexes protected by shorter length PEGs. Since the shear treatment also changes the density and morphology of the complex, the evolutional change of the complex in the short time after treatment is also shear rate dependent. For example, the sizes of the PEG_{5k}-PLL/DNA complex and its aggregates are larger in FBS 2 h after the treatment at all the studied shear rates (Fig. S3, ESI†). However, I_{ex} increases in the first region ($\dot{\gamma} \leq 50$ s^{-1}), becomes relatively stable in the second region ($70 \leq \dot{\gamma} \leq 500$ s^{-1}), and decreases in the third region ($\dot{\gamma} \geq 1000$ s^{-1}) (Fig. S4, ESI†),

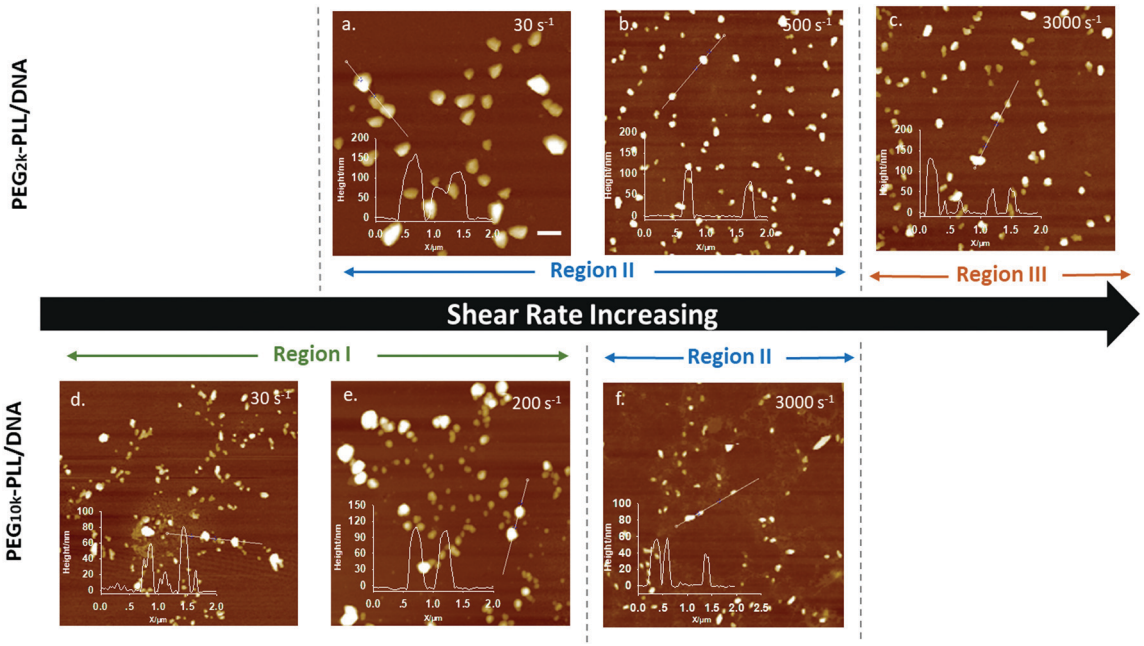

Fig. 12 AFM images and the corresponding height profile (inset) of PEG_{2k}-PLL/DNA/FBS after being sheared for 2 h at (a) 30 s^{-1}, (b) 500 s^{-1}, (c) 3000 s^{-1} and PEG_{10k}-PLL/DNA/FBS after being sheared for 2 h at (d) 30 s^{-1}, (e) 200 s^{-1} and (f) 3000 s^{-1}. Scale bar: 500 nm.

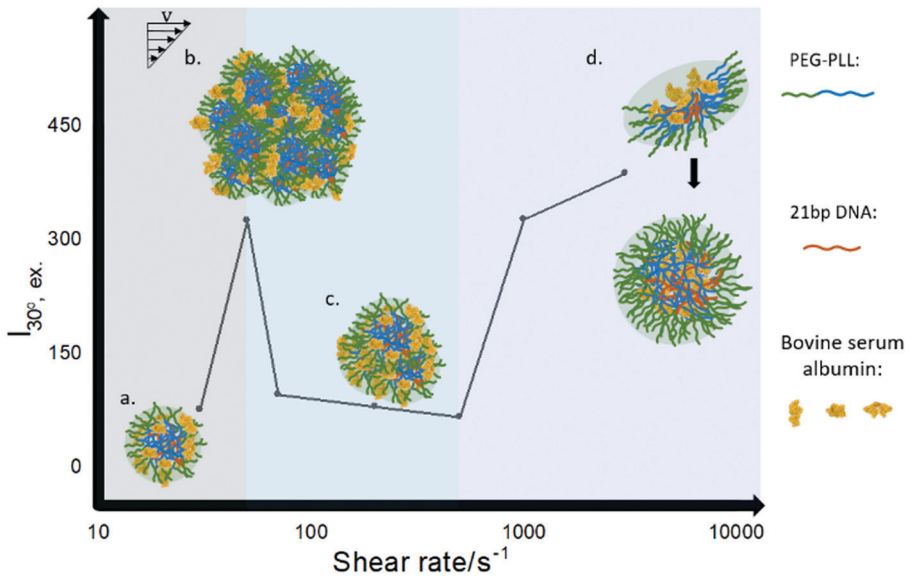

Fig. 13 Schematic display of the shear induced deformation and aggregation of the PEG–PLL/DNA complexes in the presence of serum at different shear rates.

suggesting that the complexes disturbed by PEG corona start to precipitate right after the shear stops, while the complexes that experienced from higher shear relax to a certain extent before forming precipitates.

Conclusions

The complex formed by PEG–PLL and ds-DNA exhibits multiple responses to external shear in the presence of serum. We attribute it to the featured core-corona structure of the PEG–PLL/DNA complex. The loose PEG corona is disturbed at a lower shear rate/shear time. The exposure of the charged core to the environment results in the secondary aggregation of the complex with serum. The large aggregates are broken down into small size pieces as the shear rate increases. With further increasing of shear rate to a certain level, the dense core is forced to reorganize to accommodate more serum molecules, which leads to tertiary aggregation of the complexes. If PEG cannot form a protecting corona around the complex, the first

region is missing. If the PEG corona is too stable, the last region is missing.

Our study demonstrates that the shear force determines the dynamic behaviour of gene carriers in the serum. The responsiveness of the gene carrier to the shear is related to the components and the structure of the carriers. On the one hand, the gene carries generally contain multiple components and they are fabricated into an intricate structure to overcome the obstacles along the delivery pathway; on the other hand, the shear rate in the blood stream in the human body covers a broad range, from 20 s^{-1} to 2000 s^{-1}, and is also specific to the individual. Therefore, the behaviour of the gene carriers in the blood vessels could be extremely complicated. Cross-linking the carrier through chemical bonds is an option to be free of a shear response. However, the introduction of cross-linkers, which could be toxic, and the breaking of the chemical bond upon releasing the cargo at the target site are extra concerns. The problem of designing a gene carrier which can safely go through the blood stream without reducing its transfection efficiency is still a challenge. Nevertheless, the responsiveness of the carrier to the shear rate offers an opportunity to target the carrier to certain tissues or organs if it has a specific blood flow rate.

Conflicts of interest

There are no conflicts to declare.

Acknowledgements

Financial support of this work from the National Natural Science Foundation of China (21973002) and the Beijing Natural Science Foundation (2171001) is gratefully acknowledged.

Notes and references

1 H. Yin, R. L. Kanasty, A. A. Eltoukhy, A. J. Vegas, J. R. Dorkin and D. G. Anderson, *Nat. Rev. Genet.*, 2014, **15**, 541–555.
2 I. Lostale-Seijo and J. Montenegro, *Nat. Rev. Chem.*, 2018, **2**, 258–277.
3 S. F. Dowdy, *Nat. Biotechnol.*, 2017, **35**, 222–229.
4 M. A. Mintzer and E. E. Simanek, *Chem. Rev.*, 2009, **109**, 259–302.
5 C. E. Thomas, A. Ehrhardt and M. A. Kay, *Nat. Rev. Genet.*, 2003, **4**, 346–358.
6 K. L. Douglas, *Biotechnol. Prog.*, 2008, **24**, 871–883.
7 C. Sheridan, *Nat. Biotechnol.*, 2011, **29**, 121–128.
8 R. M. Levine, C. M. Scott and E. Kokkoli, *Soft Matter*, 2013, **9**, 985–1004.
9 M. Muller, *Adv. Polym. Sci.*, 2014, **256**, V–Vi.
10 O. Boussif, F. Lezoualc'h, M. A. Zanta, M. D. Mergny, D. Scherman, B. Demeneix and J. P. Behr, *Proc. Natl. Acad. Sci. U. S. A.*, 1995, **92**, 7297–7301.
11 H. Z. Jia, S. Chen, R. X. Zhuo, J. Feng and X. Z. Zhang, *Sci. China: Chem.*, 2016, **59**, 1397–1404.
12 G. Y. Wu and C. H. Wu, *J. Biol. Chem.*, 1988, **263**, 14621–14624.
13 M. Harada-Shiba, K. Yamauchi, A. Harada, I. Takamisawa, K. Shimokado and K. Kataoka, *Gene Ther.*, 2002, **9**, 407–414.
14 D. Appelhans, H. Komber, M. A. Quadir, S. Richter, S. Schwarz, J. van der Vlist, A. Aigner, M. Muller, K. Loos, J. Seidel, K. F. Arndt, R. Haag and B. Voit, *Biomacromolecules*, 2009, **10**, 1114–1124.
15 K. M. Takeda, Y. Yamasaki, A. Dirisala, S. Ikeda, T. A. Tockary, K. Toh, K. Osada and K. Kataoka, *Biomaterials*, 2017, **126**, 31–38.
16 C. C. Su, M. T. Zhao, Z. C. Zhu, J. H. Zhou, H. Wen, Y. D. Yin, Y. Deng, D. Qiu, B. H. Li and D. H. Liang, *Macromolecules*, 2015, **48**, 756–763.
17 S. Hou, N. Ziebacz, S. A. Wieczorek, E. Kalwarczyk, V. Sashuk, T. Kalwarczyk, T. S. Kaminski and R. Holyst, *Soft Matter*, 2011, **7**, 6967–6972.
18 M. Bikram, C. H. Ahn, S. Y. Chae, M. Y. Lee, J. W. Yockman and S. W. Kim, *Macromolecules*, 2004, **37**, 1903–1916.
19 C. Brus, H. Petersen, A. Aigner, F. Czubayko and T. Kissel, *Bioconjugate Chem.*, 2004, **15**, 677–684.
20 W. J. Kim, J. W. Yockman, M. Lee, J. H. Jeong, Y. H. Kim and S. W. Kim, *J. Controlled Release*, 2005, **106**, 224–234.
21 W. J. Kim, J. W. Yockman, J. H. Jeong, L. V. Christensen, M. Lee, Y. H. Kim and S. W. Kim, *J. Controlled Release*, 2006, **114**, 381–388.
22 Y. A. Yue, F. Jin, R. Deng, J. G. Cai, Y. C. Chen, M. C. M. Lin, H. F. Kung and C. Wu, *J. Controlled Release*, 2011, **155**, 67–76.
23 M. Thibault, M. Astolfi, N. Tran-Khanh, M. Lavertu, V. Darras, A. Merzouki and M. D. Buschmann, *Biomaterials*, 2011, **32**, 4639–4646.
24 J. M. Saul, C. H. K. Wang, C. P. Ng and S. H. Pun, *Adv. Mater.*, 2008, **20**, 1091.
25 S. Boeckle, K. von Gersdorff, S. van der Piepen, C. Culmsee, E. Wagner and M. Ogris, *J. Gene Med.*, 2004, **6**, 1102–1111.
26 J. A. Champion and S. Mitragotri, *Proc. Natl. Acad. Sci. U. S. A.*, 2006, **103**, 4930–4934.
27 J. A. Champion, Y. K. Katare and S. Mitragotri, *J. Controlled Release*, 2007, **121**, 3–9.
28 S. E. A. Gratton, P. A. Ropp, P. D. Pohlhaus, J. C. Luft, V. J. Madden, M. E. Napier and J. M. DeSimone, *Proc. Natl. Acad. Sci. U. S. A.*, 2008, **105**, 11613–11618.
29 J. W. Wiseman, C. A. Goddard, D. McLelland and W. H. Colledge, *Gene Ther.*, 2003, **10**, 1654–1662.
30 Z. P. Guo, H. Y. Tian, J. L. Xia, J. Chen, L. Lin and X. S. Chen, *Sci. China: Chem.*, 2010, **53**, 2490–2496.
31 M. Ogris, S. Brunner, S. Schuller, R. Kircheis and E. Wagner, *Gene Ther.*, 1999, **6**, 595–605.
32 D. Finsinger, J. S. Remy, P. Erbacher, C. Koch and C. Plank, *Gene Ther.*, 2000, **7**, 1183–1192.
33 L. F. Brass and S. L. Diamond, *J. Thromb. Haemostasis*, 2016, **14**, 906–917.
34 L. D. C. Casa, D. H. Deaton and D. N. Ku, *J. Vasc. Surg.*, 2015, **61**, 1068–1080.
35 S. W. Schneider, S. Nuschele, A. Wixforth, C. Gorzelanny, A. Alexander-Katz, R. R. Netz and M. F. Schneider, *Proc. Natl. Acad. Sci. U. S. A.*, 2007, **104**, 7899–7903.

36 W. S. Nesbitt, E. Westein, F. J. Tovar-Lopez, E. Tolouei, A. Mitchell, J. Fu, J. Carberry, A. Fouras and S. P. Jackson, *Nat. Med.*, 2009, **15**, 665–U146.
37 A. Zanina and T. Budtova, *Macromolecules*, 2002, **35**, 1973–1975.
38 A. Pal and D. V. Khakhar, *Soft Matter*, 2019, **15**, 1979–1987.
39 M. M. Villone and P. Maffettone, *Rheol. Acta*, 2019, **58**, 109–130.
40 T. Gao, H. H. Hu and P. P. Castaneda, *Phys. Rev. Lett.*, 2012, **108**, 058302.
41 W. D. Chen, J. Z. Chen and L. J. An, *Soft Matter*, 2013, **9**, 4312–4318.
42 X. R. Sun, G. W. Wang, H. Zhang, S. Q. Hu, X. Liu, J. B. Tang and Y. Q. Shen, *ACS Nano*, 2018, **12**, 6179–6192.
43 H. Wen, Q. H. Yu, Y. D. Yin, W. Pan, S. Yang and D. H. Liang, *Biomacromolecules*, 2017, **18**, 3252–3259.
44 T. Merdan, K. Kunath, H. Petersen, U. Bakowsky, K. H. Voigt, J. Kopecek and T. Kissel, *Bioconjugate Chem.*, 2005, **16**, 785–792.
45 L. J. C. Albuquerque, A. C. Alavarse, M. C. C. da Silva, M. S. Zilse, M. T. Barth, I. C. Bellettini and F. C. Giacomelli, *Macromol. Biosci.*, 2018, **18**, 1700299.
46 J. K. W. Lam, Y. Ma, S. P. Armes, A. L. Lewis, T. Baldwin and S. Stolnik, *J. Controlled Release*, 2004, **100**, 293–312.
47 H. Sun, L. Zhou, X. L. Chen, X. Han, R. Wang and H. L. Liu, *Biopolymers*, 2016, **105**, 802–810.
48 F. Y. Dai and W. G. Liu, *Biomaterials*, 2011, **32**, 628–638.
49 S. Chen, L. Rong, Q. Lei, P. X. Cao, S. Y. Qin, D. W. Zheng, H. Z. Jia, J. Y. Zhu, S. X. Cheng, R. X. Zhuo and X. Z. Zhang, *Biomaterials*, 2016, **77**, 149–163.
50 H. Wen, Y. D. Yin, C. Huang, W. Pan and D. H. Liang, *Sci. China: Chem.*, 2017, **60**, 130–135.
51 D. Oupický, K. Howard, Č. Koňák, P. Dash, K. Ulbrich and L. Seymour, *Bioconjugate Chem.*, 2000, **11**, 492–501.

